Acta Cryst. (1977). A33, 500–508

Error Analysis in the Biophysical Applications of a Flatbed Autodensitometer*

BY MICHAEL J. ROSS† AND ROBERT M. STROUD‡

Norman W. Church Laboratory of Chemical Biology, California Institute of Technology, Pasadena, California 91125, *USA*

(*Received* 28 *June* 1976; *accepted* 18 *December* 1976)

The positional, electronic, and density accuracy of the Syntex AD-1 flatbed autodensitometer is discussed. The standard deviation of optical density measurements due to electronic noise is ±0·001 optical density units at an optical density of 0, rising to ±0·04 at an optical density of 2. No deviation from linearity in optical density measurements could be measured. During scanning, the standard deviation in position is less than 1·5 μm. Film grain noise for various films is compared and the effect of signal averaging on this noise is studied. This scanner is compared with other scanners available for accuracy of data collection from precession films.

Introduction

Many physical and biophysical techniques now in common use depend upon film methods for data collection, and to an increasing extent the analysis of these data is enhanced by, or dependent on, digital computers. The application of computer-controlled microdensitometers to the field of X-ray diffraction have ranged from digitization of single-crystal X-ray films (Arndt, Crowther & Mallet, 1968; Xuong, 1969; Nockolds & Kretsinger, 1970; Werner, 1970; and Matthews, Klopfenstein & Colman, 1972) to treatment of small-angle or large-angle X-ray scattering data from less well-ordered samples (Wooster & Fasham, 1958). The scanners are necessary for computer-aided image processing (Nathan, 1971) and image reconstruction from electron micrographs (DeRosier & Moore, 1970; Unwin & Henderson, 1975; Ross, Klymkowsky, Agard & Stroud, 1977). Additional uses are analysis of data from ultracentrifugation, electrophoretic gels, and chromatograms. These applications have generally been the province of analog microdensitometers; however, as data analysis in these fields becomes more sophisticated, the availability of computers and digitized data becomes more important.

The features of two types of computer-controlled microdensitometers have already been described in the literature. The flying-spot or cathode ray tube (CRT)-type scanner (Arndt *et al.*, 1968; Billingsley, 1971) has very high speed and flexibility, but it has a limited optical density (OD) range, relatively low positional accuracy and a high cost. The rotating drum scanner (Abrahamsson, 1966; Xuong, 1969; Nockolds & Kretsinger, 1970; and Matthews *et al.*, 1972) has relatively high speed, relatively good positional accuracy and good OD linearity. However, only flexible films with certain specific size limitations can be used, and the *x* and *y* axes of the scanner are not independently controllable.

A third type of scanner available is the flatbed scanner (Drenth, Kloosterman, van der Woude, Croon & van Zwet, 1965). This design offers excellent positional accuracy, the ability to scan any specified area of a flat object [such as electron microscope (EM) glass plates], and good OD linearity. The one drawback, for protein crystallographers alone, is the lower speed of data collection.

In this paper we describe a systematic analysis of the errors inherent in data collection with a moving-stage flatbed microdensitometer manufactured by Syntex Analytical Instruments. In order to set limits on expected errors which may be encountered when using this microdensitometer for the above-mentioned applications, we have tested some of the basic instrument parameters, specifically, positional accuracy, OD linearity, spatial resolution, stability and absolute OD accuracy. Since the accuracy of single-crystal data collection is a combination of many of the above mentioned factors (Wooster, 1964), the overall scanner performance was evaluated by analysis of X-ray precession films.

Film methods as a whole have many drawbacks. The first and most obvious is the inherent trade-off between film grain (noise) and film efficiency. Others are the lack of linearity, dynamic range, and sensitivity of films compared with electronic counting systems. Nevertheless, film is used for many experiments because; (1) there may be no alternatives, as in the cases of electron microscopy and electron diffraction where no digital electron microscope is widely available; (2) film methods often require far less capital investment than the competing methods; and (3) film offers the

* Contribution No. 5360. Supported by National Institutes of Health Grant GM-19984 and National Science Foundation Grants BMS75-04105 and GB-34881.

† National Institutes of Health Predoctoral Trainee. Present address: The Biological Laboratories, Harvard University, Cambridge, Massachusetts 02138.

‡ National Institutes of Health Career Development Awardee, US Public Health Service Grant GM-70469. Present address: Department of Biochemistry, School of Medicine, University of California, San Francisco.

advantages of spatial resolution which can lead to more efficient data collection than obtainable with present day counting systems (Arndt, Champness, Phizackerley & Wonnacott, 1973).

Experimental

Instrument description

All data were collected on a Syntex Analytical Instruments AD-1 flatbed autodensitometer interfaced to a Data General NOVA 1200 computer with 20 K words of core and a nine-track magnetic tape unit. The scanner has a useful scanning area of 15 × 15 cm, with the item to be scanned supported on a glass plate. The scanner electronics consist of computer-controlled independent x and y drive screws which drive the stage at rates up to 9·8 mm s^{-1}. during data collection. Light amplification and digitization is accomplished with a photomultiplier, preamplifier and 10-bit analog to digital (A/D) converter which is linear in transmittance; conversion to optical density is carried out digitally in the computer.

The source is a tungsten filament bulb.* Light is focused through microscope objective optics, and a rectangular defining aperture. Light transmitted through the sample is focused through a round receiving aperture of diameter approximately equal to 2·5 times the diagonal dimension of the source aperture. This arrangement allows a measurement of the specular density of the specimen. Four source aperture sizes are available: 10 × 10, 32 × 32, 55 × 109, and 109 × 219 μm. The overall gain of the optical train is adjusted by varying the high voltage on the photomultiplier. A shutter and optical fiber light pipe are used to record the photomultiplier dark current and light source intensity at each reversal of the stage direction. The scanner is capable of taking data at 6 μm intervals (1·63 kHz).†

Film processing

Kodak no-screen X-ray film was developed in Kodak liquid X-ray developer for five minutes at 20 °C with nitrogen burst agitation every twenty seconds. Electron microscope film was developed in Kodak D-19 at 20 °C for five minutes with continuous agitation. All other films were developed using Kodak D-11 developer with continuous agitation. All films were rinsed in distilled water and treated with a wetting agent (Kodak Photoflow 200).

Scanning algorithms

Data were collected using either the assembly language programs or Fortran programs provided by Syntex [the Fortran programs are modifications of the original versions written by one of us (MJR)]. This software calculates optical density as $OD = -\log[(C-D)/(R-D)]$, where C is the observed photomultiplier output at a given position, and D and R are the dark and reference values from the previous light pipe reading, respectively. At the start of each area scan, the stage is moved to the starting x,y position at slow speed and the nonscanning axis position (x)* is then corrected to its final value using a three step process. The starting position in the scanning axis (y)* is chosen to allow the scanning speed to stabilize before the initiation of data collection; this start-up distance is about 0·8 mm.

Positional accuracy in the y axis is maintained by collecting data at constant speed and by correcting for backlash using software. Areas on films are digitized by alternately moving the stage back and forth in y, taking a reference (light pipe) reading and a single step in x between each scan and the next. The three-step algorithm for x axis positioning is not carried out in between scans.

Single-crystal reflections from precession films were densitometered using the Fortran software which consists of a centering routine, a least-squares subroutine, and a data collection routine. The centering algorithm consists of manual 'joystick' movement of the film to superimpose the light spot on three axial reflections, followed by a rough calculation of an orientation matrix. This matrix is used to calculate the position of six to fifteen check reflections and each of these is scanned using the reflection scanning (spot-scan) algorithm described in Fig. 1. The centers of these reflections are calculated and then a least-squares coordinate trans-

* Although for most applications x (left to right, facing the instrument) is chosen as the nonscanning axis and y as the scanning axis, the Fortran software allows the user to change this, if desired. In this paper, the nonscanning-axis will be referred to as the x axis and the scanning axis as the y axis.

	H 0		K 0		L -12	
3130	3275		3425		2989	
2989	2592		3312		3581	
2624	2955		2886		3581	
2989	3312		2853		2561	
2853	3130		3275		3130	
3094	3464	3784	3238	3238	3275	2468
2721	3275	3743	3425	3911	3581	2853
2989	4221	4864	4707	4267	2853	2437
3702	6304	8725	8725	6379	3743	2688
3911	9910	14198	16572	9910	4605	3581
3868	13764	19396	22214	12672	4656	3542
2819	12672	17443	16572	11545	3743	3238
2721	8725	10651	11545	7795	3464	2989
3275	5254	6379	6632	5372	3425	3130
3275	4267	4811	4085	3911	3238	2468
2853	3542	4085	4041	3275	3130	2721
	3130	3425		3387		3094
	3130	3581		3130		3425
	3542	3743		2989		3425
	3464	3425		2753		3275
	2592	3743		2989		2955

Fig. 1. Single-crystal spot scan. The figure shows the positions of the optical densities (× 10 000) which were collected around a typical strong reflection. The interior of the circled area was used for intensity integration and the surrounding area for background estimation. Data are from a scan of a 17° precession (*h0l* layer) X-ray diffraction photograph of trypsinogen. This scan was collected using the assembly-language software.

* The power supply for the light bulb was modified to allow operation at either an increased voltage of 6·3 V or at the standard 5 V; this increase in light intensity was useful when the 10 μm spot was used.

† A modification of the frequency response characteristics of the preamplifier was implemented in order to change the roll-off frequency from 400 to 2000 Hz.

form matrix is computed for use by the data collection subroutine. Individual spot-scans centered about each calculated reciprocal lattice point on the film are carried out and from these individual scans, backgrounds and integrated intensities for each reflection are calculated (Fig. 1). If Laue streaks are present, the program allows the option of collecting backgrounds only on those sides of the reflection through which the streaks do not pass. The film OD's are corrected for nonlinearity effects by using the logarithmic correction determined by Morimoto & Uyeda (1963): for Kodak no-screen film the equation is

$$OD_{corr} = -7{\cdot}823 \log_e [(8{\cdot}333 - OD_{obs})/8{\cdot}333]$$

where OD_{corr} is the corrected OD. This correction was chosen as an alternative to the parabolic correction used by Matthews *et al.* (1972) because it could be used for data collected with only one film per pack, whereas the parabolic correction is based on scaling two or more films together. Parameter data files containing the indices of check reflections, information on space group and other data collection parameters, are stored on disk or tape and need be generated only once for each crystal structure being studied.

Data reduction

Data reduction was carried out on a Data General NOVA 800 computer with 32 K words of core, a 2·4 M byte disk, a Syntex Analytical Instruments floating-point processor, two magnetic tape units and a Versatec 1100A matrix printer/plotter. Data from area scans were treated in several ways: (1) a gray-level histogram (Billingsley, 1971), displaying the number of pixels (digital picture elements) present in the image at each optical density, was calculated (for example, see Fig. 2*a*); (2) the image was linearly integrated over either x or y with the resultant average OD plotted *vs* position along the other axis (for example, see Fig. 2*b*); (3) the digitized data were displayed as a half-tone image on the matrix plotter (for example, see Fig. 2*c*).

From the histogram, the minimum, maximum, mean, mode, and median OD's were calculated as were the OD's between which 95·4% of the observations occurred. The latter would represent two standard deviations from the mean if the data obeyed a Gaussian distribution and will be referred to in this paper as 2σ levels, even when applied to non-Gaussian distributions.

Precession film data were corrected for both Lorentz and polarization factors (Waser, 1951); all symmetry-equivalent reflections were averaged, and those with large standard deviations were flagged; first, second and third films from the same pack (when available) were scaled linearly together on medium strength reflections. Reflections with OD's greater than 2·3 were not used.

This scaling procedure allowed us to verify the efficacy of the logarithmic scaling procedure by plotting $OD_{film\ 1}$ *vs* $OD_{film\ 2}$. No deviation from linearity on this plot was found, indicating the correctness of the logarithmic scaling parameters.

Positional accuracy

A razor blade (Wilkinson platinum) was set on the glass stage with the edge perpendicular to the scan axis. The razor blade was scanned using a scanner step size of 10 μm and the 219 μm length of the 219×109 μm spot size. The transmittance (counts) was plotted *vs* position for each scan. The counts should decrease linearly as the spot is slowly eclipsed with any positional errors reflected as deviations from linearity. The very beginning and end of the graphs curve, because of the diffraction limits of the optics, to give an overall sigmoidal shape to the plot. The central portion of each plot (from 20% to 80% transmittance) was fitted to a least-squares line and the deviation from linearity was used as a measure of positional accuracy along the scanning axis.

The nonscanning axis positioning was checked using a similar technique. In this case, the razor-blade edge was placed parallel to the scanning axis and the stage was iteratively moved (10 μm steps in the nonscanning axis direction) so as to eclipse the light spot. The transmittance readings were plotted and subjected to least-squares analysis as above. The nonscanning-axis positioning was tested using the two different algorithms supplied by Syntex: (1) slewing to position followed by a three-step positional adjustment; and (2) stepping the nonscanning axis between successive scans. The long dimension of the 219×109 μm spot was used for these tests since it allows data collection over longer distances in the region of the edge.

Spatial resolution

The projected light spot size, although a major factor, is not the only parameter affecting scanner resolution. In the AD-1, lens imperfections, the frequency response of the detection and digitizing circuitry, and the absolute diffraction limitations of the optics (Billingsley, 1971) could lead to resolution lower than that theoretically obtainable for a given spot size. Instead of trying to measure or calculate each of these individual parameters and risk overlooking others, it was decided simply to measure the sine-wave response function of the optical system (Perrin, 1960). In this test, parallel Ronchi rulings (engine-enscribed 50% black, 50% clear glass rulings, Edumund Scientific, 50, 100, 200, and 300 cycles/inch) were scanned* with each of the four spot sizes; they were scanned with the direction of the ruled lines either parallel or perpendicular to the scanning-axis. At some low ruling frequency where the light spot is much smaller than the objects (*i.e.* rulings) to be resolved, an essentially perfect rendition of the pattern would be realized; however, as the ruling fre-

* Sine-wave patterns should ideally be used, but are difficult to manufacture. Perrin (1960) points out that square waves, *i.e.*, alternating light and dark bars are a satisfactory substitute.

quency approaches the resolution limits of the densitometer, the scanner response decreases, and at some limiting high spatial frequency no response at all should be detectable.

Electronic noise

The glass plate was removed from the scanner stage and the optics were refocused. An area containing 200×200 OD measurements (pixels) was densitometered and recorded on magnetic tape using the area-collection algorithm. Total noise was measured as a function of: (1) spot size; (2) photomultiplier voltage, and (3) readings from the photomultiplier (ψOD).*

Total scanner noise

In order to assay for increased noise caused by dust or small scratches on the glass, an area (200×200 pixels) of the glass plate was scanned using the area-collection algorithm for each of the four spot sizes and a statistical analysis of the scanner noise was carried out as described above. Since image reconstructions of electron micrographs are done using the Fourier transform of digitized images, the Fourier components of the scanner noise were calculated using a two-dimensional fast Fourier algorithm (Ross *et al.*, 1977).

Long-term stability

The dark current, light-pipe reference reading, and light through the optical system were sampled every eight hours for three days. The test was carried out using the 109×55 μm spot with a clean glass stage and no stage movement. During this period of three days, the room temperature was allowed to vary from 20 °C to 30 °C. The filament in the source was left on continuously.

Photomultiplier fatigue

The scanner was designed such that the photomultiplier would be kept in a state of constant fatigue (low sensitivity) by 'flashing' it with the bright reference beam at the conclusion of each y scan. A 'worst-case' test of the effectiveness of this procedure was designed: long (longer than two seconds) scans of high ψOD were digitized to see whether photomultiplier sensitivity changed within a given y scan.

This test was carried out by scanning seven-centimeter-long sections (y-scan time of about seven seconds) of a glass optical wedge (absolute OD 0·5 to 3·0; total length was 22·5 cm; manufactured by Joyce–Loebl). Scans up the wedge started at low relative optical density and ended at higher relative optical density. The reverse was true for scans down the wedge. The integrals of the OD's on the scans up and the scans down the wedge were compared. If the photomultiplier were to change in sensitivity during the y scans, we would expect the integral of the OD's on the scans up the wedge to be larger than the integral of the OD's on the scans down the wedge; a dark (high OD) section of the scan at the scan start would presumably cause the OD measurements for the rest of the scan to be anomalously low (photomultiplier too sensitive).

Absolute OD accuracy

Gelatin neutral density filters of OD 0·10, OD 0·50, and OD 0·90 (Eastman Kodak) were scanned both separately and in pairs. The average measured density of each filter was corrected to an absolute OD value by subtracting the measured OD of the glass plate.

OD linearity

Two independent tests for OD linearity were employed. In the first test a razor blade (Wilkinson platinum) was placed at an angle of approximately 0·5° to the y axis. The scanner was positioned such that the light spot did not intersect the razor blade at the start of a y scan and had completely disappeared by the end of it; the razor blade was so scanned for each of the four spot sizes. The razor blade was examined microscopically and found to have an edge roughness of about 0·5 μm r.m.s. The scans were displayed as counts (transmittance) *vs* position; these plots bore a strong resemblance to the sigmoidal plots described under *Positional accuracy* above.The central portions of the curves (from 20 to 80% transmittance) were fitted to a least-squares line and the deviations from linearity were measured.

The second test involved use of a linear glass density wedge (see above). Although care had to be taken that defects in the wedge were not being measured, this test was used to extend the results of the razor-blade test to the full range of densities measurable by the scanner. The glass wedge was placed on the densitometer bed and scanned using all four spot sizes and the full range of photomultiplier voltage settings.

Two different seven-centimeter sections of the wedge were used for all tests to estimate the contributions due to nonlinearity in the wedge. For each test, data from 20 scans were averaged to reduce the noise.

Film noise

Unexposed samples of each film type were processed, areas of each film were digitized using the area-scan algorithm for various spot sizes, and the OD's in the digitized area were statistically analyzed. The scanned area was then further processed by averaging integral numbers of rows and/or columns of pixels to test the effect of signal averaging on film grain noise.

Results

Positional accuracy

The maximum deviation in scanning-axis position was 4·6 μm. The standard deviation was $\pm 1{\cdot}5$ μm from

* ψOD is the calculated OD corresponding to the digital output of the AD-1 electronics. It is not necessarily the same as the true OD of the sample being densitometered. The ψOD can be manipulated by changing the gain of the photomultiplier, changing the lamp power supply voltage, or by changing the scanner apertures.

the calculated position. Since the x-axis positioning between scans was handled differently than the x-axis positioning at the start of a scan sequence (see *Experimental* section), the errors in these two processes were measured separately. The maximum deviation found in the x-axis positioning algorithm used at the start of spot or area scans was 2·2 μm. The standard deviation of positioning was $\pm 1{\cdot}4$ μm. Between y scans, the x positioning was found to have a maximum deviation of 2·9 μm and a standard deviation of $\pm 0{\cdot}9$ μm.

Spatial resolution

The scans of the glass rulings were analyzed with gray-level histograms (Fig. 2*a*). The ΔOD between the 2σ levels in the histograms were normalized ($\Delta\text{OD} = 3$ was deemed to be 100% response), and displayed as a function of ruling frequency for each spot size (Fig. 3). Substantial loss (>30%) of the high spatial frequency content of the image occurred whenever the scanner spot was larger than one third the size of the object to be resolved. This falloff can be corrected by real-space or Fourier-space filtering of the digitized image.

Since the normalized ΔOD never fell below 5% even when the spot size exceeded the ruling spacing by several times, we examined both half-tone images (Fig. 2*c*) and linearly integrated images (Fig. 2*b*) of each digitization. In all cases, image contrast reversal* (Andrews, 1970) started to appear in these images as the normalized ΔOD fell below 20%. Thus, when the scanner is to be used for image analysis, care should be taken not to densitometer images with high-amplitude features smaller than the spot size, even if their resolution is not desired, because the appearance of false features in the digital image will be the result.

Noise

The noise level of the densitometer was measured by the standard deviation of the densitometer readings from the median OD with the glass stage removed, and characterized as a function of several variables. There was no change in the noise level as the photomultiplier voltage was changed from 400 to 1100 V (ψOD was kept constant), nor was there any detectable dependence on spot size (ψOD also constant). In both of these cases, the noise level ($\psi\text{OD} = 0$) was found to have standard deviations of from $\pm 0{\cdot}0015$ OD to $\pm 0{\cdot}0025$ OD. However, as might be expected in a system which is digitized as a linear function of transmittance, the noise level increased exponentially with increasing ψOD (see Fig. 4). The scanner exhibited a very low noise level at low optical densities, increasing to one with a standard deviation of $\pm 0{\cdot}066$ OD ($\pm 3\%$) for measurements at OD 2·2.

* Image contrast reversal is a condition which occurs during digitization of images in which black areas appear white and white areas appear black. It is a result of the sampling of the densitometer and is also called 'false resolution' since features appear resolvable but are not accurate representations of the object being densitometered.

When the glass plate used for supporting films was replaced in the scanner and these measurements repeated, no change in the standard deviations of the measurements from the median were observed, although the maximum deviations from the median OD increased to a value of 0·02 OD ($\psi\text{OD} = 0$) for all spot sizes. This represented increases in maximum deviations from the median of up to five times at low optical densities.

This densitometer noise was analyzed by Fourier series to determine if the noise was white or whether components of specific x and y frequencies were important. The two-dimensional power spectrum of the noise (Fig. 5*a*) was displayed. At ψOD less than 1·0, two features were identifiable. First, with all apertures, one feature appeared in transformations: a strip of higher-magnitude Fourier coefficients which were zero

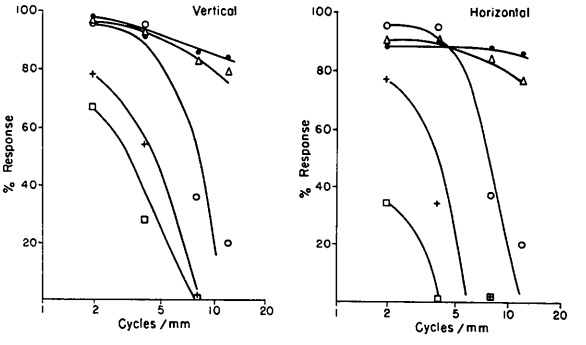

Fig. 3. Sine-wave response test. Normalized 2σ deviations from gray-level histograms (Fig. 2*a*) are plotted as a function of the ruling frequency in cycles/mm. The width of each stripe (black or clear) on the rulings is half of the spatial frequency of the rulings. The data for resolution in both the horizontal (x-axis) and vertical (y-axis) directions are plotted for each of the spot sizes. The following symbols are used: □ = 219 × 219 μm spot; + = 109 × 55 μm spot; ○ = 32 × 32 μm spot; ● = 10 × 10 μm spot. The scanner response was also measured with the 10 × 10 μm light spot using the receiving aperture normally used with the 32 × 32 μm spot (△).

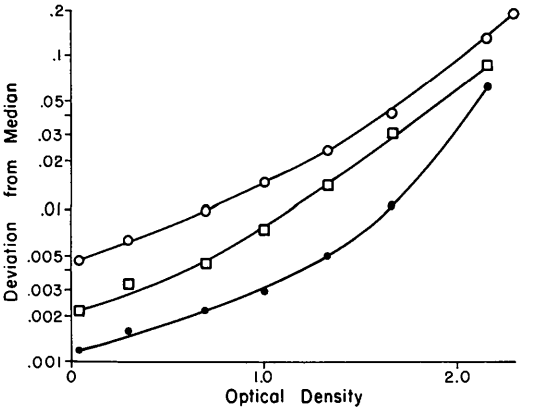

Fig. 4. Electronic noise. Deviations from the median ψOD are plotted as a function of ψOD: ○ = maximum deviation from the median; □ = 2 standard deviations from the median; ● = 1 standard deviation from the median.

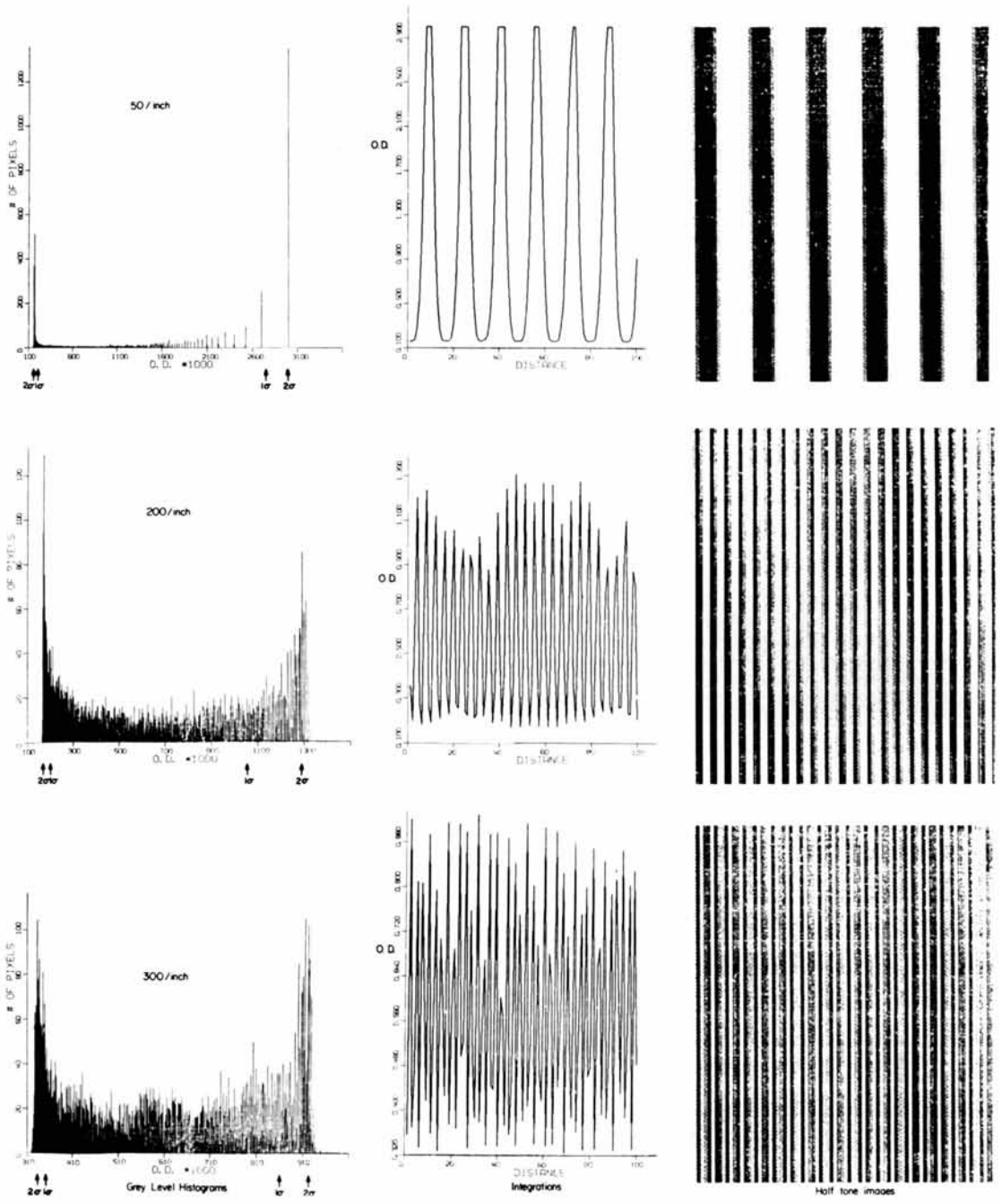

(*a*) (*b*) (*c*)

Fig. 2. Analysis of the area scans of rulings (black-white) at various spatial frequencies. The scanner light spot size was 32 × 32 μm. A decrease in scanner response can be noted as the ruling spatial frequency is increased. (*a*) Gray-level histograms show the number of pixels (OD measurements) present in the image at each optical density. 1σ and 2σ levels are noted on the histograms. (*b*) Linear integrations of the digitized images show image degradation as the frequency is increased. (*c*) Half-tone images are examined to check for fidelity of the digitized image.

[*To face p.* 504

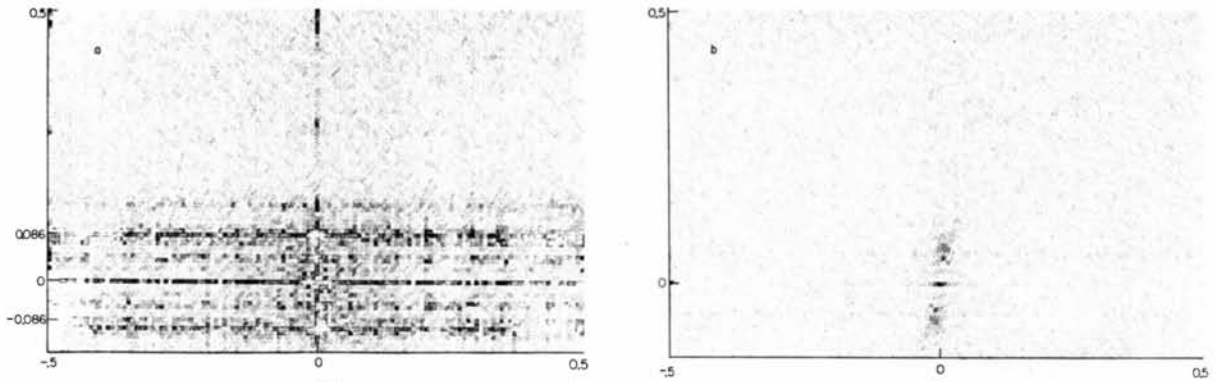

(*a*) (*b*)

Fig. 5. Half tone two-dimensional Fourier transform scanner noise displayed 100× normal image intensity to accentuate the pattern. The vertical axes on these plots correspond to the transformed x axis of the scanner, and the horizontal axis to the y axis. Frequency in [scan area]$^{-1}$ is noted in the figure. (*a*) The 10 μm light spot and receiving aperture was used The horizontal line at zero frequency is due to variations of the average OD of each scan from changes in the reference reading; other lines are due to vibration resonances and only appear when the smallest aperture is used. (*b*) 10 μm light spot, 32 μm receiving aperture. Reference and dark-current readings were held constant for the OD calculations. Note the disappearance of most of the lines caused by vibration and also the zero-order term in x.

order in x appeared. These higher-magnitude terms seemed evenly distributed along y (see Fig. 5). This effect was traced to the method by which the densitometer calculated OD (see *Experimental* section): the OD's within each y scan were being calculated relative to the light-pipe (reference) reading for that scan. Therefore the noise from the statistical variations in the reference readings appeared as zero-order Fourier terms along the y axis. To correct for this, the area-scan algorithm was changed to allow calculation of OD assuming a constant reference and dark current for all y scans; these values were determined at the start of the scan of the entire area. This procedure eliminated the strip of larger Fourier coefficients (Fig. 5) but had one potential drawback: long-term drift in OD readings could result from thermal or light-bulb drift. These errors would, however, be automatically filtered out if a Fourier space-masking procedure such as that used in image reconstruction were carried out.

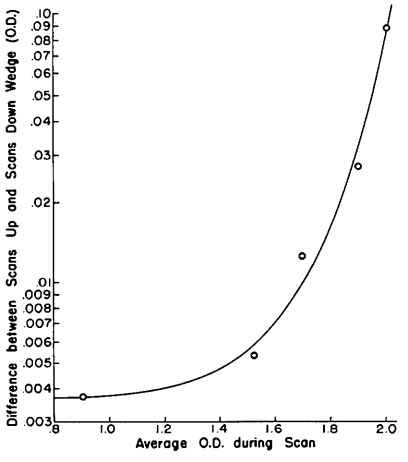

Fig. 6. Photomultiplier fatigue. The average OD for scans down a glass OD wedge (higher to lower OD) were subtracted from the average OD for scans up the same wedge. The resulting hysteresis is plotted *vs* the average ψOD of the wedge. The photomultiplier sensitivity is shown to change during the y scans.

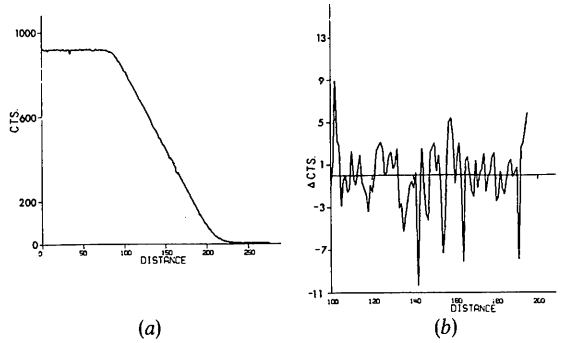

(*a*) (*b*)

Fig. 7. Linearity: oblique scan of a razor blade. The razor blade was placed at an angle of ~0·5° to the y axis. (*a*) The resulting scan was plotted as counts (transmittance) *vs* position. (*b*) The linear portion of (*a*) was fitted to a least-squares line and the difference between the observed data and the line was plotted.

The second phenomenon observed from Fourier analysis of the noise became most obvious when using the 10×10 μm source aperture. Relatively strong repetitive noise (thirty times that seen using the 32×32 μm spot) was observed with the smaller spot (Fig. 5*a*) and traced to mechanical vibration of the DC pulse motors used to drive the stage. The noise terms were large enough to interfere with image reconstructions of electron micrographs scanned with the 10×10 μm spot. We found that they could be almost eliminated (reduced seventyfold) by using a larger receiving aperture than usual. When the receiving aperture normally used with the 32×32 μm spot was used with the 10 μm-square light spot, only a 5 % reduction in resolution could be measured (Fig. 3), implying that the reduction in noise was not coupled with a substantial decrease in performance. A similar reduction in the systematic noise level found with the 32×32 μm source spot was achieved by use of a larger receiving aperture (that normally used with the 109×55 μm spot).

Stability and hysteresis

The long-term stability of the scanner was tested to determine the efficacy of the pseudo-double beam optics used. Over a period of four days with ambient temperatures of 20 to 30 °C, the drift in transmittance was 5·8 %, but the corrected optical densities varied by only 0·01 OD. The photomultiplier sensitivity was found to increase during long (longer than two seconds) scans of high ψOD (*i.e.* low photomultiplier current). This led to an observed hysteresis in the scans of the optical wedge (see Fig. 6). This effect was found to be a function of the average ψOD during a scan, but not a function of the photomultiplier voltage. A large increase in photomultiplier sensitivity during the scans was noted as the average ψOD rose above 1·6 (Fig. 6).

OD accuracy and linearity

The measured OD of calibrated neutral density filters varied linearly with OD rating of the filters such that the measured OD was approximately 4·5 % high. This is not surprising since the filters are calibrated on a densitometer which measures transmitted light over a 180° angle of acceptance (diffuse density) whereas the AD-1 measures transmitted light scattered over an angle of about 4° (specular density). This specular density is always greater than or equal to the diffuse density since any light scattered at an angle of greater than 4° cannot be recorded.

The deviation from optical linearity as measured by the oblique scan of the razor blade was ± 3 counts for the largest spot size (Fig. 7*a*). (Transmittance was digitized in the range of 0–1023 counts.) The measured errors increased with decreasing spot size to ± 13 counts for the 10×10 μm spot. Visual inspection of the difference plots (deviation from least-squares line, Fig. 7*b*) showed that most of the measured deviation was due to high-frequency noise which was traced to roughness in the razor-blade edge.

An inherently less noisy test of linearity was carried out using a glass OD wedge. The results were analyzed as a function of ψOD, spot size, and photomultiplier voltage (Fig. 8*a*, *c*). Root-mean-square (standard) deviations of the difference curve (deviations from the least-squares line) were the same as measured in the electronic noise test for any ψOD range from 0 to 2·8 (Fig. 8*b*,*d*). At low average optical densities, nonlinearities of 0·005 OD should have been detectable but were not seen.

Small low-frequency variations in the difference curve were observable even though they were too small to affect the statistical analysis of the noise (Fig. 8*b*, *d*). These features were traced to imperfections in the wedge rather than to nonlinearities in the optical system. This follows from the observations that the low-frequency variations remained invariant as ψOD, spot size, or photomultiplier voltage were changed but moved in position when different areas of the wedge were analyzed.

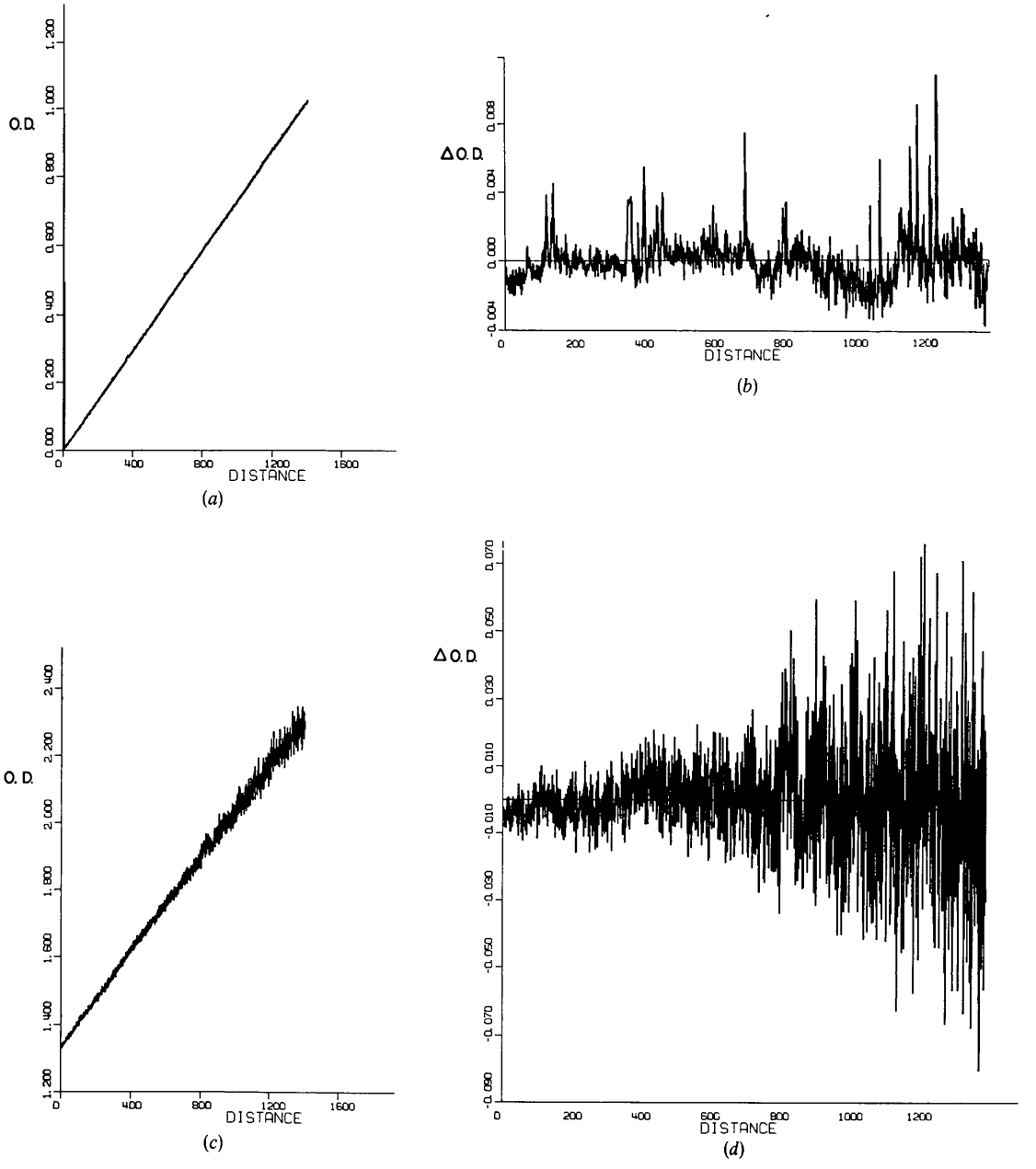

Fig. 8. Linearity: scan of an OD wedge. The wedge was scanned with different starting ψOD's. Twenty scans were averaged for each graph. All graphs are of the same section of wedge using the 219 × 109 μm spot. (*a*) Low average OD. Note the low overall noise level. (*b*) Same as (*a*) with least-squares line subtracted. (*c*) High average OD. Note the higher average noise level. (*d*) Same as (*c*) with least-squares line substracted.

Film noise

A table of maximum and standard deviations (from the median OD) for processed unexposed films was compiled to act as a reference for noise estimation in images recorded on these films (Table 1).

Table 1. *Film grain noise*

Film	Deviation (OD) Maximum	Standard
High-Contrast Lantern-Slide Plates*[a]	0·15	0·0011
Electron Microscope Film*[a]	0·08–0·26	0·0056
Electron Microscope Film*[d]	0·07–0·31	0·0056
Type 4127 Commercial Film*[a]	0·14	0·010
Type 4125 Copy Film*[a]	0·069	0·014
Plus-X Pan*[a]	0·11	0·019
Royal Pan*[a]	0·17	0·025
Cronex X-ray Film†[a]	0·39	0·040
Industrial G‡[a]	0·12	0·010
Industrial G‡[b]	0·07	0·007
No-Screen X-ray Film*[a]	0·29	0·044
No-Screen X-ray Film*[b]	0·17	0·013
No-Screen X-ray Film*[c]	0·078	0·012

* Eastman Kodak. † E. I. DuPont. ‡ Ilford.

(*a*) 32 × 32 μm spot.
(*b*) 109 × 55 μm spot.
(*c*) 219 × 109 μm spot.
(*d*) 10 × 10 μm spot.

The results for signal-to-noise enhancement by averaging neighboring picture elements are shown in Fig. 9. The higher spatial frequency components of the film grain noise would be expected to be reduced by this averaging while the longer-range components of the noise would remain. The noise level (especially as measured by the maximum deviation) is seen to drop with averaging, but a surprising amount of grain noise is not eliminated. Although the standard deviations for electron microscope film (about ±0·004 OD) are much lower than for X-ray film (about ±0·03 OD) when no averaging has been performed, the relative improvement in the noise level after averaging is similar for the two films. The implication of this result is that superposition techniques used in image enhancement and radial integration techniques used in processing low-angle X-ray films have limited effectiveness in reducing noise.

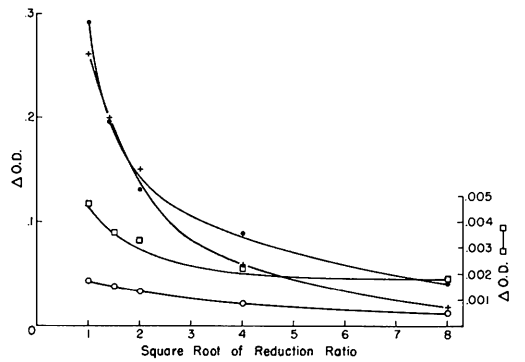

Fig. 9. Effect of data averaging on film noise. Unexposed films and the resulting density array reduced in size by averaging neighboring pixels. Noise (deviation from median OD of the film) is plotted as a function of (reduction ratio)$^{1/2}$ where reduction ratio = (image area before averaging)/(image area after averaging). ● = maximum deviation for Kodak no-screen X-ray film; ○ standard deviation for Kodak no-screen X-ray film; + maximum deviation for Kodak electron micrograph film; vertical scale is at the left of the figure. □ standard deviation for electron microscope film; vertical scale is at the right of the figure for these data only. Spot size was 32 × 32 μm for all data.

Single-crystal X-ray data collection

The setup, centering, and least-squares process can be accomplished in less than five minutes using the software provided by Syntex. The rate at which individual reflections could be densitometered varied from two to seven seconds per reflection. Sixteen spots of four different average OD's were measured 100 times each using the same orientation matrix. (The matrix was calculated once at the start of the test using the software described in the *Experimental* section.) The individual calculated intensities $[I_j(k)]$ for each reflection were compared with the average intensity for that reflection $[\bar{I}(k)]$ as a residual R_1:

$$R_1 = \frac{\sum_{j=1}^{100} |I_j(k) - \bar{I}(k)|}{\sum_{j=1}^{100} |I_j(k)|}.$$

R_1 was then averaged over the four reflections of similar intensity. The results are summarized in Table 2.

Table 2. *Reproducibility of the measurement of single-crystal diffraction data from the same film*

Reflection strength	R_1^* (%)
Weak† (0·2 OD)	0·8
Intermediate† (0·8 OD)	0·45
Strong† (2·0 OD)	0·5
No reflection† (0 OD)	4·0
Entire film‡ (All reflections $>2\sigma$ above noise)	3·2

* R_1 as defined in the text.
† Same orientation matrix.
‡ New orientation matrices calculated for each of five measurements of the same film.

The reproducibility varied from 0·45% to 0·8% for reflections with average OD's greater than 0·2 OD above backgrounds and rose to 4% when an equivalent area of the film containing a systematically absent reflection was similarly treated. This increase in percentage error can be ascribed to film grain noise since the film grains being measured are on the order of 0·1 μm and are much smaller than either the positional precision of the scanner or the spot size.

Table 3. *Comparison of symmetry-related reflections*

R^*_{sym} (%)	Maximum OD	Scanner type	
5·1	1·2	Flying spot	Arndt *et al.* (1968).
6·0	2·0	Rotating drum	Xuong (1969).
4·4 (typical film)	2·5	Rotating drum	Matthews *et al.* (1972).
3·6 (best film)	2·5	Rotating drum	
4·3 (typical film)	2·3	Flatbed	This work.
2·0 (best film)	2·3	Flatbed	

* R_{sym} as defined in the text.

Symmetry-related reflections on the same film were compared using R_{sym} (Arndt *et al.*, 1968):

$$R_{sym} = \frac{\sum_i^{sym} |I_i(h) - \bar{I}(h)|}{\sum_i^{sym} |I_i(h)|}$$

The results of the best film and of typical films are compared with published results derived from precession data collected on other scanners (see Table 3).

Discussion

The Syntex AD-1 has been found to have an average error in position of less than 1·5 μm in each dimension. It has a spatial resolution limited only by the light spot chosen (as small as 10×10 μm). No nonlinearity of the light-sensing circuitry could be measured above the electronic noise level, and the variations in OD due to electronic noise increased logarithmically with OD as would be expected since the digital electronics were linear in transmittance. The 2σ noise level was $\pm 0{\cdot}002$ OD at a measured OD of 0 increasing to only $\pm 0{\cdot}04$ OD at OD 2. With appropriate precautions, there were no limitations placed on the use of the scanner for Fourier image analysis using any spot size.

The instrument exhibited excellent long-term (hours to days) stability even with wide temperature fluctuations. The one notable problem with the scanner occurred only when scanning long stretches of high optical density film (ψOD > 2). Under these conditions the photomultiplier sensitivity changed as much as 5% during the scan.

The noise properties of the films examined (Table 1) varied widely. The higher sensitivity films such as Royal Pan and X-ray film had far higher film grain noise than the lower sensitivity films such as Type 4127 or electron microscope film. The measured film noise can be used to set reliability limits on digitized data collected using these films.

The measurement of intensities from single-crystal X-ray films requires accuracy in both positional and density measurements. Several researchers (Arndt *et al.*, 1968; Xuong, 1969; Matthews *et al.*, 1972; Nockolds & Kretsinger, 1970) have described results from both flying-spot and drum autodensitometers when used for this purpose. These instruments collect data at the rate of about 0·5 to 0·6 seconds per reflection. Peak OD's of reflections of up to 1·2 (Arndt *et al.*, 1968) can be used with the flying-spot densitometer; Matthews *et al.* (1972) found that OD's of up to 2·5 could be accommodated with application of appropriate corrections for film nonlinearity. Data collected on the AD-1 scanner had equivalent or better precision than the above-mentioned instruments (see Tables 2 and 3) with a data collection speed of two to seven seconds per reflection and a setup time of less than five minutes per film.

In conclusion, the AD-1 proved to be a satisfactory instrument for use in collecting single crystal data from X-ray films. It is also capable of the positional and electronic precision necessary in more exacting applications such as digitizing electron micrographs.

References

ABRAHAMSSON, S. (1966). *J. Sci. Instrum.* **43**, 931–933.

ANDREWS, H. C. (1970). *Computer Techniques in Image Processing*, p. 37. New York: Academic Press.

ARNDT, U. W., CHAMPNESS, J. N., PHIZACKERLEY, R. P. & WONNACOTT, A. J. (1973). *J. Appl. Cryst.* **6**, 457–463.

ARNDT, U. W., CROWTHER, R. A. & MALLET, J. F. W. (1968). *J. Phys. E*, **1**, 510–517.

BILLINGSLEY, F. C. (1971). *Advanc. Opt. Electron Microsc.* **4**, 127–159.

DEROSIER, D. J. & MOORE, P. B. (1970). *J. Mol. Biol.* **52**, 355–369.

DRENTH, J., KLOOSTERMAN, D., VAN DER WOUDE, J., CROON, H. C. & VAN ZWET, L. C. M. (1965). *J. Sci. Instrum.* **42**, 222–224.

MATTHEWS, B. W., KLOPFENSTEIN, C. E. & COLMAN, P. M. (1972). *J. Phys. E*, **5**, 353–359.

MORIMOTO, H. & UYEDA, R. (1963). *Acta Cryst.* **16**, 1107–1119.

NATHAN, R. (1971). *Advanc. Opt. Electron Microsc.* **4**, 85–126.

NOCKOLDS, C. E. & KRETSINGER, R. H. (1970). *J. Phys. E*, **3**, 842–846.

PERRIN, F. H. (1960). *J. SMPTE*, **69**, 239–249.

ROSS, M. J., KLYMKOWSKY, M. W., AGARD, D. A. & STROUD, R. M. (1977). Submitted to *J. Mol. Biol.*

UNWIN, P. N. T. & HENDERSON, R. (1975). *J. Mol. Biol.* **94**, 425–440.

WASER, J. (1951). *Rev. Sci. Instrum.* **22**, 563–568.

WERNER, P. E. (1970). *Acta Cryst.* A **26**, 489–491.

WOOSTER, W. A. (1964). *Acta Cryst.* **17**, 878–882.

WOOSTER, W. A. & FASHAM, F. A. L. (1958). *J. Sci. Instrum.* **35**, 153–156.

XUONG, NG-H. (1969). *J. Phys. E*, **2**, 485–489.